

Fluid interfaces with very sharp tips in viscous flow

Sylvain Courrech du Pont^a and Jens Eggers^b

^aLaboratoire Matière et Systèmes Complexes, UMR CNRS 7057, Université Paris Diderot, 10, rue Alice Domon et Léonie Duquet, 75205 Paris cedex 13, France; ^bSchool of Mathematics, University of Bristol, Fry Building, Woodland Road, Bristol BS8 1UG, United Kingdom

This manuscript was compiled on November 11, 2020

1 When a fluid interface is subjected to a strong viscous flow, it tends
 2 to develop near-conical ends with pointed tips so sharp, their radius
 3 of curvature is undetectable. In microfluidic applications, tips can
 4 be made to eject fine jets, from which micron-sized drops can be
 5 produced. Here we show theoretically that the opening angle of the
 6 conical interface varies on a logarithmic scale as function of the dis-
 7 tance from the tip, owing to non-local coupling between the tip and
 8 the external flow. Using this insight we are able to show that the tip
 9 curvature grows like the exponential of the square of the strength
 10 of the external flow, and to calculate the universal shape of the in-
 11 terface near the tip. Our experiments confirm the scaling of the tip
 12 curvature as well as of the interface's universal shape. Our analytical
 13 technique, based on an integral over the surface, may also have far
 14 wider applications, for example treating problems with electric fields,
 15 such as electrosprays.

Free surface flows | singularities | selective withdrawal | microfluidics

1 In many problems of science and engineering, or in daily
 2 life, one is confronted with fluid interfaces subject to strong
 3 external flows. For example, consider a bubble rising in a
 4 viscous fluid (1) (such as in a shampoo bottle), emulsions of
 5 drops or bubbles being stirred (2, 3), a viscous layer being
 6 withdrawn from near an interface (4), or two fluids meeting in
 7 a microfluidic channel (5).

8 In Fig. 1 we show three typical situations: at the top, a
 9 viscous liquid (light) flows out through a circular hole at the
 10 bottom of the picture, deforming the interface between liquid
 11 and air - a flow geometry known as selective withdrawal (6–
 12 8). The interface is focused into a near-conical shape, which
 13 ends in a tip so small, it can no longer be resolved by optical
 14 means. Therefore, in the inset we show profiles obtained from
 15 a numerical simulation: as the tip is plotted with increasing
 16 resolution (decreasing a), the observed opening angle increases.
 17 This is a reflection of the logarithmic variation of the interface
 18 slope, which is the key feature of the solution described below.

19 In the middle we see a drop of liquid, whose viscosity is
 20 much smaller than that of the outer liquid, being drawn apart
 21 by an extensional flow. Once more, very sharp tips are formed
 22 at the ends of the drop, and the ends appear conical. At the
 23 bottom, a conical interface is produced when a stream of oil is
 24 forced by water in a microfluidic assembly (5, 9, 10). However,
 25 now a liquid thread escapes from the tip (a phenomenon
 26 called tipstreaming (11)), whose subsequent decay is a means
 27 of producing micron-sized droplets in a highly reproducible
 28 fashion (12) of interest for chemical analysis and in soft matter
 29 research.

30 Similar conical structures, known as Taylor cones, appear
 31 when a liquid is placed in a strong electric field (13–15). How-
 32 ever, the Taylor cone is generally unstable, and a tiny jet
 33 is emitted from its tip (11, 16–18), akin to the tipstreaming
 34 phenomenon described above. This has led to a vast number
 35 of applications in spraying and materials processing (19, 20),

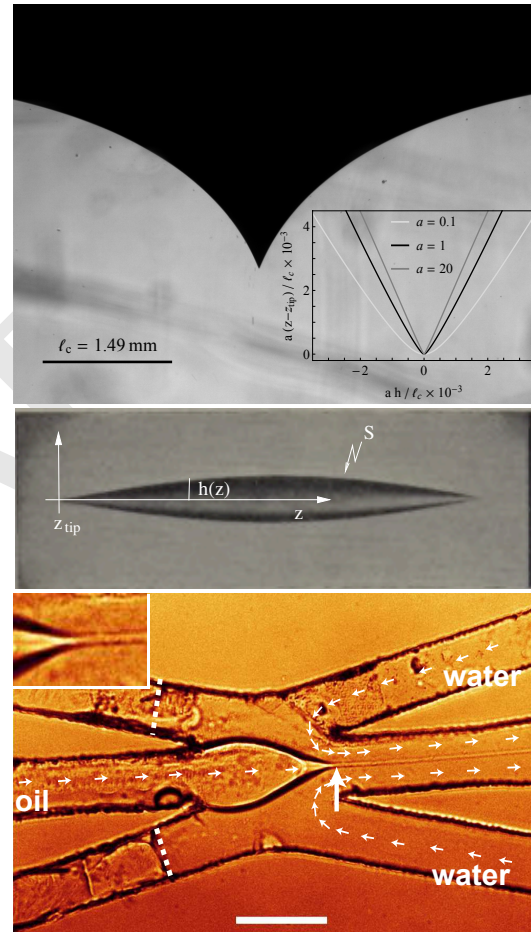


Fig. 1. Top: A liquid-air interface is deformed into a sharp tip as the fluid below escapes through a hole at the bottom (8); ℓ_c is the capillary length. The dimensionless source strength (flow rate q) is $\chi = q\eta/(\ell_c^2\gamma) = 6.31$, where η the dynamic viscosity, and γ the surface tension. The local capillary number (details below) is $Ca_{\text{tip}} = 1.64$. The inset shows closeups of the tip found from a numerical simulation of the experiment: as one zooms in, the opening angle increases. Middle: A low-viscosity drop in an extensional flow generated by four rollers (2), with capillary number $Ca = GR_d\eta/\gamma = 0.7$, and unperturbed drop radius $R_d = 0.25\text{cm}$, where G is the extension rate of the flow. Bottom: A stream of oil is being forced into a sharp tip by water flowing in the reverse direction at a junction of small channels (12). A jet a few microns thick is ejected from the tip (see inset). The scale bar represents $75\mu\text{m}$.

36 but the fundamentals of how a Taylor cone leads to secondary
37 structures has not been understood properly.

38 Almost a century ago, G.I. Taylor set up a research program
39 to understand the production and stirring of emulsions (2, 21),
40 by considering drops subjected to simple external forcing,
41 as seen in Fig. 1. After stirring, very small drops of about
42 1/100 the size of the original drop can be observed (2), which
43 can be attributed to the ejection of small threads, similar
44 to those shown at the bottom of the figure. Taylor later
45 developed a theory for the shape of slender drops of small or
46 negligible viscosity (22), which predicted conical ends with
47 tips of vanishing size, violating the assumption of smoothness,
48 on which continuum theory is based (23).

49 Later refinements of Taylor’s theory (24) show that it breaks
50 down near the tips. Other theoretical proposals for drop
51 shapes also exhibit singular tips (24, 25). Our later numerical
52 calculations (26) suggest a finite curvature at the tips, which
53 grows exponentially with the square of the external flow speed.
54 It remains to understand this issue of singular tips theoretically,
55 and to calculate the true shape near the ends. This task has
56 hitherto proven impossible, since it represents a fully non-
57 linear, three-dimensional free-surface problem, for which few
58 analytical methods of solution exist. In particular, a slender-
59 body or lubrication type approach fails here, since the end is
60 not a slender shape.

61 The axisymmetric geometry we consider is particularly
62 significant, since it represents “optimal” focusing of the flow.
63 In the two-dimensional analogue of the same problem, the
64 interface shape is a cusp (27, 28), whose tip traces out a line
65 in three dimensions. Since this involves focusing along a whole
66 line, it is much less efficient than focusing on a single point,
67 as in the present problem. As a result, the curvature only
68 increases exponentially with the flow strength in the quasi
69 two-dimensional case, instead of the exponential of the square.
70 Our analytical calculation of the curvature of an axisymmetric
71 tip establishes theoretically that steady flows with surface
72 tension are always smooth, although rounding may occur on
73 very small scales only.

74 The idea of our analysis is that the region near the tip is
75 on a scale very different from the bulk of the flow. Thus if
76 we introduce the distance $\zeta = (z - z_{\text{tip}})\kappa_m$ from the tip (see
77 Fig. 1, middle), made dimensionless with (twice) the mean
78 curvature of the tip κ_m , the radius $h(z)$ of an axisymmetric

interface can be written in the form

$$h(z) = \kappa_m^{-1} H(\zeta), \quad [1]$$

where $H(\zeta)$ should be a universal similarity solution, inde-
pendent of the geometry or of the external flow. In (26) we
provided numerical evidence for Eq. (1), comparing $H(\zeta)$ cal-
culated from a drop in extensional flow, and from a selective
withdrawal configuration. Below we calculate the similarity
function $H(\zeta)$ analytically for large ζ , which corresponds to
the limit of large κ_m at a small but constant distance from
the tip. We then use this to calculate the scaling of the tip
curvature as function of the local flow strength.

Asymptotic analysis near the tip. To calculate the profile and
the flow near the ends, we consider the simplest case of axisym-
metric viscous (Stokes) flow, with vanishing viscosity inside.
Even if inertia becomes important on a large scale, this will
still be a correct description locally, where the local Reynolds
number is small, i.e. viscous forces are much stronger than
inertial forces. An axisymmetric cross section is a good approx-
imation even if the external flow is not axisymmetric (29, 30),
for example in a shear flow. A finite viscosity fluid inside the
tip eventually leads to a tipstreaming bifurcation (22, 31), but
we will be describing the regime before this occurs, yet tips
have become very sharp.

Instead of solving the flow equations in the bulk, with
boundary conditions applied at the free surface, we use the
equivalent boundary integral description (32), which is formu-
lated on the free surface alone, and which has proven extremely
effective addressing free surface problems numerically with
very high resolution (26, 32, 33). However, this technique is
very unwieldy as an analytical tool, since the surface to be in-
tegrated over is unknown a priori. Here we break new ground
by using the boundary integral technique to find analytical
solutions, using the fact that the interface slope is changing
very slowly.

The integral equation to be solved for the velocity $\mathbf{v}(\mathbf{x}_1)$
on the surface S (see Fig. 1, middle, more details in *Materials
and Methods*) is (32)

$$\frac{\mathbf{v}(\mathbf{x}_1)}{2} = \mathbf{v}^{(ext)}(\mathbf{x}_1) - \int_S \kappa(\mathbf{x}_2) \mathbf{J} \cdot \mathbf{n} d\sigma_2 - \int_S \mathbf{v}(\mathbf{x}_2) \cdot \mathbf{K} \cdot \mathbf{n} d\sigma_2. \quad [2]$$

Velocities are written in units of the capillary speed $v_c \equiv \gamma/\eta$,
with γ the surface tension and η the dynamic viscosity. In
Eq. (2), $\mathbf{v}^{(ext)}(\mathbf{x}_1)$ is an externally imposed velocity, κ
the mean curvature, and \mathbf{n} the outward normal. The kernel $\mathbf{J} \cdot \mathbf{n}$
is the velocity at \mathbf{x}_1 , generated by a point force at \mathbf{x}_2 in Stokes
flow, and $\mathbf{K} \cdot \mathbf{n}$ is the corresponding stress tensor at \mathbf{x}_1 .

Since the flow is axisymmetric, one can perform the az-
imuthal integration explicitly (32), and choose the dimen-
sionless distance ζ from the tip as the integration variable.
Transforming to the logarithmic variable $l = \ln \zeta$, we obtain
from Eq. (2)

$$\frac{\mathbf{v}(l_1)}{2} = v_{\text{tip}} \mathbf{e}_z + \mathbf{v}^{(J)} - \int_{-\infty}^{\ln(L\kappa_m)} \mathbf{v}(l_2) \zeta_2 \mathbf{k}(l_1, l_2) dl_2, [3]$$

$$\mathbf{v}^{(J)}(l_1) = - \int_{-\infty}^{\ln(L\kappa_m)} \zeta_2 (\kappa(l_2)/\kappa_m) \mathbf{j}(l_1, l_2) dl_2, \quad [4]$$

where L is a characteristic size of the setup, such as a drop
size, and $v_{\text{tip}} = v_z^{(ext)}(z_{\text{tip}})$ is the external velocity at the tip.

Significance Statement

Turn a shampoo bottle upside down, and the rising bubble develops a very sharp tip at its rear. Similar conical structures have been observed placing a drop in an electrical field. Owing to the significance of such structures in chemical processing or in geophysics, they have been studied for almost a century. Here we present a consistent analysis of the shape near the tip in flow. We show that the size of the tip always remains finite, but decreases so rapidly in size with the flow strength, that it may be considered zero for practical purposes.

S. C. du P. performed selective withdrawal experiments; J. E. developed the theory and wrote the manuscript

The authors have no conflict of interest to declare

^b To whom correspondence should be addressed. E-mail: jens.eggerts@bris.ac.uk

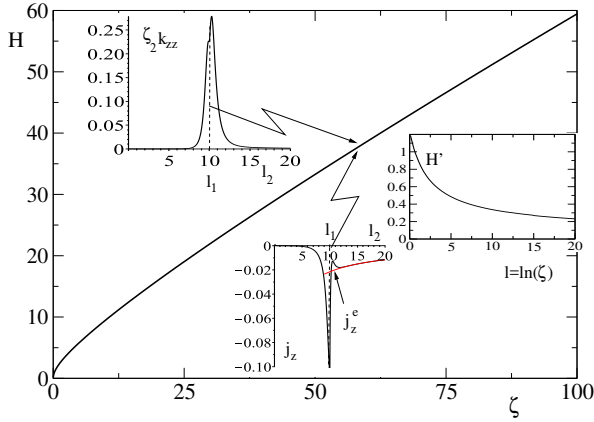


Fig. 2. Schematic representation of our treatment of Eq. (6). The self-similar profile $H(\zeta)$ has a slope H' which changes on a logarithmic scale, see inset. Integrands like $\zeta_2 k_{zz}$ are peaked at $l_2 = l_1$, except j_z , which decays like j_z^e for large l_2 .

Namely, taking a cone of slope s_2 as the interface, one finds that for $\Delta \rightarrow \infty$

$$j_z(l_1, l_2) \rightarrow j_z^e \equiv -\frac{s_2^2(1-s_2^2)}{4(1+s_2^2)^{3/2}} \approx -\frac{s_2^2}{4}, \quad [7]$$

where j_z^e is shown as the red line in the plot of j_z in Fig. 2. In the same limit of small slopes, $\zeta_2 \kappa / \kappa_m \approx 1/s_2$; thus the integrand of $v_z^{(J)}$ in Eq. (4) is $\zeta_2(\kappa/\kappa_m)j_z \approx -s_2/4$. On the other hand, for $\Delta \rightarrow -\infty$, $j_z(l_1, l_2)$ vanishes rapidly (cf. Fig. 2), and we obtain

$$v_z^{(J)} \approx \frac{1}{4} \int_{l_1}^{\ln(L\kappa_m)} s(l_2) dl_2. \quad [8]$$

Clearly since $s \propto 1/\sqrt{l_2}$, this integral makes a contribution $\propto \sqrt{\ln(L\kappa_m)}$ from its upper limit. Once this has been removed by balancing it against v_{tip} in Eq. (6), we anticipate that $v_z \propto \sqrt{l_1}$ from the lower limit.

Now we compute the other integrals in the same spirit as integrals over cones, but using the fact that the remaining kernels are localized about $\Delta \approx 0$, and decay for large Δ . Thus since $\mathbf{j}(l_1, l_2) = \mathbf{j}(s_1, \Delta)$ for a conical interface, we can approximate

$$v_r^{(J)} \approx (\zeta_1 \kappa(l_1) / \kappa_m) \int_{-\infty}^{\infty} j_r(s_1, \Delta) d\Delta = 0,$$

which is confirmed by an expansion of $j_r(s_1, \Delta)$ for small s_1 .

The kernels $\mathbf{k}(l_1, l_2) \approx \mathbf{k}(s_1, \Delta)$ can be treated in the same way. Beginning with z -component of Eq. (6),

$$K_1 \equiv \int_{-\infty}^{L\kappa_m} \zeta_2 k_{zz} v_z(l_2) dl_2 \approx v_z(l_1) \int_{-\infty}^{\infty} \zeta_2 k_{zz}(s_1, \Delta) d\Delta,$$

where we have used, as illustrated in Fig. 2, that $\zeta_2 k_{zz}$ is strongly peaked, so that $v_z(l_2)$ varies little over width of the peak. The remaining integral (the area of the peak) can be shown to be $1/2$ to leading order in an expansion for small s_1 (see *Materials and Methods*); thus $K_1 \approx v_z(l_1)/2$. In the same vein,

$$K_3 \equiv \int_{-\infty}^{L\kappa_m} \zeta_2 k_{zr} v_r(l_2) dl_2 \approx v_r(l_1) \int_{-\infty}^{\infty} \zeta_2 k_{zr}(s_1, \Delta) d\Delta.$$

Now the integral is $\approx s_1/2$ to leading order, which becomes small, and K_3 can be neglected compared to K_1 .

Coming to the r -component of Eq. (6), to a first approximation we have

$$K_4 \equiv \int_{-\infty}^{L\kappa_m} \zeta_2 k_{rr} v_r(l_2) dl_2 \approx v_r(l_1) \int_{-\infty}^{\infty} \zeta_2 k_{rr}(s_1, \Delta) d\Delta.$$

To leading order, the value of the last integral is $-1/2$, so that $K_4 \approx -v_r/2$; but this cancels $v_r/2$ on the left, and we have to go to the next order, which yields $K_4 \approx v_r(l_1)(-1/2 + s_1^2/4)$. The remaining component is

$$K_2 \equiv \int_{-\infty}^{L\kappa_m} \zeta_2 k_{rz} v_z(l_2) dl_2 \approx v_z(l_1) \int_{-\infty}^{\infty} \zeta_2 k_{rz}(s_1, \Delta) d\Delta,$$

but the integral is again zero to leading order, and even the next order vanishes. To capture the leading nonzero contribution, we expand $v_z(l_2) = v_z(l_1) + v'_z(l_1)\Delta + \dots$, using that k_{rz}

The kernels \mathbf{j} and \mathbf{k} correspond to $\mathbf{J} \cdot \mathbf{n}$ and $\mathbf{K} \cdot \mathbf{n}$ in Eq. (2), integrated over θ , and written in units of the tip curvature κ_m .

The integrands in Eq. (3) and Eq. (4) are now invariant under a scale transformation: if the surface were a perfect cone of slope s , the integrands would be functions of s and $\Delta = l_2 - l_1$ alone. Thus if all integrals were convergent in the limit $L\kappa_m \rightarrow \infty$, each term in Eq. (3) would be a function of s alone, and a cone would result as a (similarity) solution to the flow equations. However, as first pointed by Taylor (22), and confirmed by Buckmaster (24), such a conical solution does not exist. Indeed, we will see that the z -component of $\mathbf{v}^{(J)}$ in Eq. (4) is in fact divergent for $L\kappa_m \rightarrow \infty$, so L cannot be eliminated from the problem. Instead, we must keep the upper limit in Eq. (4) finite, and cancel the resulting contribution against the external velocity v_{tip} , introducing an intrinsic coupling between the external flow and the local behavior at the tip.

The key idea of our approach is to suppose that the interface has the form (cf. Fig. 2):

$$H(\zeta) = \zeta s(\ln \zeta) \equiv \zeta s(l), \quad [5]$$

where $s(l)$ is a local slope, which varies on a logarithmic scale. We will show below that for large l (far from the tip), which is the asymptotic behavior which interests us, $s(l) \propto 1/\sqrt{l}$, i.e. the slope becomes small, as shown in the inset of Fig. 2. In doing so, we are always in the limit $\zeta \ll L\kappa_m$, and hence the inner solution near the end applies. If we write Eq. (3) in the form

$$\frac{1}{2} \begin{pmatrix} v_z \\ v_r \end{pmatrix} = \begin{pmatrix} v_{\text{tip}} + v_z^{(J)} - K_1 - K_3 \\ v_r^{(J)} - K_2 - K_4 \end{pmatrix}, \quad [6]$$

in evaluating the dominant contribution to each term we can assume the integral to be over a cone of constant slope (since $s(l)$ is varying very slowly), which is a tractable problem.

Our treatment of Eq. (6) is illustrated in Fig. 2: to find $v_{z/r}$ at a point $l_1 = \ln(\zeta_1)$, according to Eq. (3) and Eq. (4), we have to perform an integral over l_2 . However, as shown for the example of $\zeta_2 k_{zz}$, integrands are peaked at $l_2 = l_1$, and hence to leading order the contribution to K_1 is proportional to $v_z(l_1)$, multiplied by the area of the peak. The exception is the integral over j_z , which decays very slowly for large l_2 .

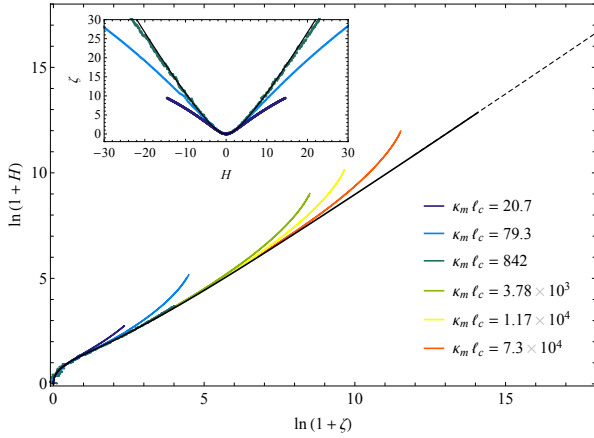


Fig. 3. Comparison between the similarity solution $H(\zeta)$ as predicted by theory (black solid line), and six different experimental data sets for different values of $\kappa_m \ell_c$, rescaled according to Eq. (1) (colored lines); $\ell_c = \sqrt{\gamma/(\rho g)} = 1.49\text{mm}$ is the capillary length. The main panel shows all six experimental data sets on a logarithmic scale, the inset only the first three sets on a linear scale. The dashed line is the asymptotic behavior Eq. (9) with $l_0 = 2.55$. For the first three experimental profiles, κ_m has been measured directly, (colored dots in Fig. 4), for the profiles with the highest tip curvatures, κ_m has been calculated from a numerical simulation (colored pluses in Fig. 4).

an extensional flow (26); the constant of integration l_0 was adjusted to match with the numerical profile. The major conclusion from Eq. (10) is that the pointed ends seen for example in Fig. 1 only appear conical since s is nearly constant over an observable range of scales, but this opening angle will change when the scale of observation is changed, and one zooms into the tip.

The theoretical tip similarity solution $H(\zeta)$ (black solid line) is compared in Fig. 3 to six experimental data sets from a selective withdrawal experiment, described in detail in (8) (colored lines). A container 3 cm wide is half filled with silicone oil of viscosity $\eta = 30\text{ Pa s}$ and surface tension $\gamma = 2.13 \times 10^{-2}\text{ Nm}^{-1}$. The liquid is evacuated through a circular sink hole of 1 mm diameter in a solid plate, at a constant flow rate of $q = 9.97 \times 10^{-9}\text{ m}^3/\text{s}$, but replenished at a rate which is slightly smaller, so that the distance between the hole and the mean liquid level decreases adiabatically, over a period of several hours.

As the liquid-air interface comes closer to the sink hole, it is increasingly deformed. We record the distance z_t between interface tip and the hole, as well as the shape of the interface. The experimental cell is lit from behind, so that light is refracted away by the interface, whose cross section appears black (cf. Fig. 1), top. The measured interface shape (colored lines) has been rescaled according to Eq. (1), with tip curvatures given in the figure. The crossover between the similarity solution $H(\zeta)$ and the outer solution, which is shaped by the sink flow out of the container, takes place at a fixed outer scale $z - z_{\text{tip}}$. Thus to increase the range of the similarity variable ζ over which to compare to the experiment, one has to increase the tip curvature.

For the first three profiles of Fig. 3, the tip curvature κ_m has been measured directly by interpolating the tip region. The teal curve with the highest curvature shows significant noise, as it has been zoomed in to the limit of our resolution. To be able to compare to theory over a larger range, we included three profiles with a much larger tip curvature, focusing on the far field. The tip sizes of these profiles have become so small, that they are below our optical resolution. Instead, we calculate κ_m from a full numerical simulation of the flow equations, which matches closely the experimental geometry. We can argue on the basis of Fig. 4 below that the numerical estimates of the curvature are very reliable.

To compute the tip curvature κ_m analytically, we insert Eq. (10) into the First of Eq. (9) to find to leading order

$$-\frac{\sqrt{l}}{2} \approx -\text{Ca}_{\text{tip}} + \frac{1}{4} \int_l^{\ln(L\kappa_m)} \frac{dl_2}{\sqrt{l_2}}, \quad (11)$$

where the local capillary number $\text{Ca}_{\text{tip}} = -v_{\text{tip}}$ is the dimensionless z -velocity at the tip. From this we find $\text{Ca}_{\text{tip}} \approx \sqrt{\ln(L\kappa_m)}/2$, and thus

$$\kappa_m \propto L^{-1} \exp(4\text{Ca}_{\text{tip}}^2), \quad (11)$$

which is the main result of this paper. For Eq. (11) to be valid, Ca_{tip} needs to be sufficiently large so that there is an appreciable range over which s follows the scaling Eq. (10). Owing to the faster-than-exponential growth of κ_m , Eq. (11) shows that while the curvature always remains finite, it can easily reach microscopic dimensions even at moderate values of the capillary number. For example, taking the drop in the

is peaked around $\Delta = 0$. Thus an improved approximation becomes

$$K_2 \approx v'_z(l_1) \int_{-\infty}^{\infty} \Delta \zeta_2 k_{rz}(s_1, \Delta) d\Delta \approx -v'_z(l_1) \frac{s_1}{2}$$

to leading order.

This completes the necessary calculations of all the integrals. Next we will interpret Eq. (6) as a dynamical system for $s(l)$, $v_z(l)$ and $v_r(l)$.

Flow equations and scaling. To summarize, Eq. (6) becomes to leading order, putting $l_1 = l \equiv \ln \zeta$,

$$v_z = v_{\text{tip}} + \frac{1}{4} \int_l^{\ln(L\kappa_m)} s(l_2) dl_2, \quad 0 = s v'_z/2 - v_r s^2/4. \quad [9]$$

The contribution v_{tip} of the external flow cancels against the contribution from the upper limit of the $v_z^{(J)}$ integral, as we see below. However, we first calculate $s(l)$ to leading order. To close the system Eq. (9), we use that streamlines must be parallel to the free surface, and thus $v_r/v_z = H' = s + s' \approx s$. Differentiating the First of Eq. (9) with respect to l , we find $v'_z = -s/4$, and substituting into the second equation gives $v_r = -1/2$. This corresponds to the familiar result (34, 35) $-v_c/2$ for the rate of collapse of a cylindrical cavity, remembering that velocities have been made dimensionless with the capillary speed v_c . It follows that $v_z = -1/(2s)$ from the kinematic condition, leading to $s' = -s^3/2$. Solving, we find the asymptotic solution far from the tip (but still in the self-similar region) to be

$$s = (l - l_0)^{-1/2}, \quad v_r = -\frac{1}{2}, \quad v_z = -\frac{(l - l_0)^{1/2}}{2}, \quad [10]$$

consistent with the previous assumption of small slopes for $l \rightarrow \infty$. In Fig. 3, Eq. (10) (dashed line) is found to be in excellent agreement with $H(\zeta)$ as calculated from Eq. (1) (solid line), using a full numerical simulation of a drop in

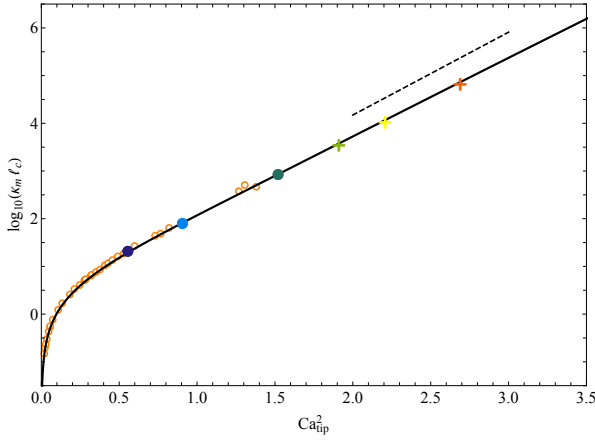


Fig. 4. The dimensionless tip curvature $\kappa_m \ell_c$, as function of the square of the local capillary number Ca_{tip} , based on the *unperturbed* velocity at the tip. The solid line is a numerical simulation (details in (26)), parameters the same as Fig. 1 (top). The open orange circles are the experimental measurements, applying no adjustable parameters. The filled circles correspond to the measured curvature of the first three profiles of Fig. 3, the pluses are the curvatures for the last three profiles, based on the numerical simulation. The dashed line has a slope of $a = 4 / \ln 10$, corresponding to the theoretical prediction Eq. (11).

middle of Fig. 1, Eq. (11) would predict a radius of curvature of about 10^{-89} m! This shows that while the tip itself is often too small to observe, what is experimentally relevant is the slow variation of the slope described by our asymptotic theory Eq. (10).

In Fig. 4 we test Eq. (11) against experiment (circles) and simulation (solid line). As the capillary number increases, the logarithm of the curvature, plotted as function of the square of the capillary number at the tip, quickly converges toward a straight line. The dashed line has a slope of $4 / \ln 10$, which is the asymptotic prediction of Eq. (11), and is seen to agree very well with both simulation and experiment. It can be shown (36) that the slight over prediction of the slope can be traced to a slow variation of the *prefactor* in Eq. (11) on the capillary number.

The orange circles in Fig.4 come from measurements of the tip curvature in the selective withdrawal geometry for the same parameters as in Fig. 3. The external velocity at the tip was calculated from the flow field of a point source inside a solid wall, evaluated at z_t . The black solid line is the result of a numerical simulation performed using the boundary integral method (26). The simulation assumes a point source in a solid wall, unbounded in the horizontal direction (instead of a finite experimental cell), an approximation which works very well, except far from the center (26). No adjustable parameters were applied to achieve the near-perfect agreement between simulation and experiment. The colored solid circles are also obtained from direct measurements of the tip curvature, and correspond to the first three profiles of Fig. 3. The pluses have been picked out from the solid line, and mark the curvatures of the last three profiles of Fig. 3.

Conclusions. In this paper, we have given the first analytical description of axisymmetric interface tips, created by a converging viscous flow. The shape of the interface near the tip is universal, independent of flow conditions. The tip curvature always remains finite, but increases dramatically with flow strength. Thus although surface tension always keeps

the interface smooth, the continuum hypothesis will in many cases fail in practice. Moreover, it follows that the numerical solution of free-surface problems places extreme demands on the spatial resolution. Our analytical solution can be used to provide effective boundary conditions on intermediate scales, to drastically reduce the necessary numerical effort. Numerical calculations agree well with our experiments, which resolve the tip size down to a few microns.

Using the theoretical framework established in this paper, we hope to address the important issue of tipstreaming, used to produce colloidal drops (5, 12), and studied numerically in (37, 38). The same is true for a much wider class of flows involving electric fields, where the analogous flow is known as the cone-jet mode (11, 39). In (12), it was shown that in a suitable microfluidic geometry (see Fig. 1, bottom), the transition to tipstreaming is of second order, i.e. the ejected thread can be arbitrarily thin. Thus we expect the transition between a tipstreaming state and a closed tip to be continuous, which means that previous theories of tipstreaming, based on slender-body theory (40, 41), suffer from the same shortcomings as for a tipped state. By adding an inner fluid to our description, we expect to be able to include the thread into our theory, finally being able to address the tipstreaming problem in a consistent fashion.

Materials and Methods

The idea of the boundary integral Eq. (2), is to use the linearity of the Stokes equation to write the velocity as a superposition of an externally imposed velocity field $\mathbf{v}^{(ext)}$, and the velocity $\mathbf{v}^{(J)}$ produced by surface tension. The latter can be seen as coming from a collection of point forces of strength $\gamma \kappa \mathbf{n}$, distributed over the surface S . This makes $\mathbf{v}^{(J)}$ a superposition of *Stokeslets* \mathbf{J} , integrated over the free surface S , with $\gamma \kappa \mathbf{n}$ as a weight.

The kernels in the boundary integral description Eq. (2) are (32)

$$J_{ij}(\mathbf{r}) = \frac{1}{8\pi} \left[\frac{\delta_{ij}}{r} + \frac{r_i r_j}{r^3} \right], \quad K_{ijk}(\mathbf{r}) = -\frac{3}{4\pi} \frac{r_i r_j r_k}{r^5}, \quad [12]$$

where $\mathbf{r} = \mathbf{x}_1 - \mathbf{x}_2$, so that $\mathbf{J} \cdot \mathbf{f}(\mathbf{x}_2)$ is the velocity at \mathbf{x}_1 , generated by a point force \mathbf{f} at \mathbf{x}_2 , and $\mathbf{K} \cdot \mathbf{f}(\mathbf{x}_2)$ is the stress at \mathbf{x}_1 . The factor $1/2$ on the left-hand side of Eq. (2) and the second integral over the stress $\mathbf{K} \cdot \mathbf{n}$ corrects for the jump in viscosity between the two phases.

Putting $\mathbf{x}_1 = (y_1, 0, x_1)$, $\mathbf{x}_2 = (y_2 \cos \theta, y_2 \sin \theta, x_2)$, and $\bar{\mathbf{n}} = (-h'(z), 1)$, we can perform the integration with respect to the azimuthal angle θ :

$$\mathbf{j} = y_2 \int_0^{2\pi} \mathbf{J} \cdot \bar{\mathbf{n}} d\theta_2, \quad [13]$$

and analogously for \mathbf{K} , yielding the kernels \mathbf{j} and \mathbf{k} in Eq. (3) and Eq. (4). They result in well-known expressions (32) involving elliptic integrals in terms of the (logarithmic) coordinates l_1, s_1 and l_2, s_2 .

The entries in Eq. (6) are calculated by performing the integrals over l_2 assuming a conical interface with slope $s_1 = s(l_1)$. This results in integrals over the kernels, such as $\zeta_2 k_{zz}(s_1, \Delta)$ for the case of K_1 , but as a function of $\Delta = l_2 - l_1$ alone. The dominant contribution to the integral comes from a central region of size s_1 . At higher orders, contributions for $\Delta \geq 1$ also need to be taken into account, but can be disregarded here.

To capture contributions at scale s , we put $\xi = \Delta/s$ and expand the kernel:

$$\zeta_2 k_{zz} = K_1^{(-1)}(\xi) s^{-1} + K_1^{(0)}(\xi) + \dots$$

Here $K_1^{(-1)}(\xi)$ is an even function, which is expressible in terms of the elliptic integrals $E\left(2/\sqrt{4+\xi^2}\right)$ and $K\left(2/\sqrt{4+\xi^2}\right)$ (42).

Thus the integral becomes

$$\int_{-\infty}^{\infty} \zeta_2 k_{zz} d\Delta = \int_{-\infty}^{\infty} K_1^{(-1)} d\xi + O(s^2) = \frac{1}{2} + O(s^2),$$

as shown by an explicit calculation. The remaining integrals to calculate $K_2 \dots K_4$ can be evaluated in a similar fashion, expanding the integrand in s at constant ξ .

ACKNOWLEDGMENTS. We are grateful to Howard Stone for useful comments on the manuscript.

1. Manga M, Stone HA (1993) Buoyancy-driven interactions between two deformable viscous drops. *J. Fluid Mech.* 256:647–683.
2. Taylor GI (1934) The formation of emulsions in definable fields of flow. *Proc. Roy. Soc. London A* 146:501.
3. Bentley BJ, Leal LG (1986) An experimental investigation of drop deformation and breakup in steady, two-dimensional linear flows. *J. Fluid Mech.* 167:241.
4. Lister JR (1989) Selective withdrawal from a viscous two-layer system. *J. Fluid Mech.* 198:231–254.
5. Anna SL (2016) Droplets and bubbles in microfluidic devices. *Annu. Rev. Fluid Mech.* 48:285.
6. Cohen I, Nagel SR (2002) Scaling at the selective withdrawal transition through a tube suspended above the fluid surface. *Phys. Rev. Lett.* 88:074501.
7. Case SC, Nagel SR (2007) Spout states in the selective withdrawal of immiscible fluids through a nozzle suspended above a two-fluid interface. *Phys. Rev. Lett.* 98:114501.
8. Courrech du Pont S, Eggers J (2006) Sink flow deforms the interface between a viscous liquid and air into a tip singularity. *Phys. Rev. Lett.* 96:034501.
9. Anna SL, Bontoux N, Stone HA (2003) Formation of dispersions using “flow focusing” in microchannels. *Appl. Phys. Lett.* 82:364.
10. Utada AS, Fernandez-Nieves A, Stone HA, Weitz DA (2007) Dripping to jetting transitions in coflowing liquid streams. *Phys. Rev. Lett.* 99:094502.
11. Montanero JM, Gañán-Calvo AM (2020) Dripping, jetting and tip streaming. *Rep. Prog. Phys.* 83:097001.
12. Dong J, Meissner M, Eggers J, Seddon AM, Royall CP (2018) Opposed flow focusing: evidence of a second order jetting transition. *Soft Matter* 14:8344.
13. Taylor GI (1964) Disintegration of water drops in an electric field. *Proc. Roy. Soc. London A* 280:383.
14. Li H, Halsey TC, Lobkovsky A (1994) Singular shape of a fluid drop in an electric or magnetic field. *Europhys Lett.* 27:575.
15. Stone HA, Lister JR, Brenner MP (1999) Drops with conical ends in electric and magnetic fields. *Proc. Roy. Soc. Lond. A* 455:329.
16. Taylor GI (1969) Electrically driven jets. *Proc. Roy. Soc. London A* 313:453.
17. Gañán-Calvo AM (1997) Cone-jet analytical extension of Taylor’s electrostatic solution and the asymptotic universal scaling laws in electrospinning. *Phys. Rev. Lett.* 79:217.
18. Eggers J, Villermaux E (2008) Physics of liquid jets. *Rep. Progr. Phys.* 71:036601.
19. Bailey AG (1988) *Electrostatic Spraying of Liquids*. (Wiley).
20. Reneker DH, Yarin AL (2008) Electrospinning jets and polymer nanofiber. *Polymer* 49:2387–2425.
21. Taylor GI (1932) The viscosity of a fluid containing small drops of another fluid. *Proc. Roy. Soc. London A* 138:41.
22. Taylor GI (1964) Conical free surfaces and fluid interfaces in *Proceedings of the 11th International Congress of Applied Mathematics, Munich (Germany)*, ed. Görtler H. (Springer, Heidelberg), pp. 790–796.
23. Batchelor GK (1967) *An Introduction to Fluid Dynamics*. (Cambridge University Press, Cambridge).
24. Buckmaster JD (1972) Pointed bubbles in slow viscous flow. *J. Fluid Mech.* 55:385.
25. Sherwood JD (1981) Spindle-shaped drops in a viscous extensional flow. *Math. Proc. Camb. Phil. Soc.* 90:529.
26. Eggers J, Courrech du Pont S (2009) Numerical analysis of tip singularities in viscous flow. *Phys. Rev. E* 79:066311.
27. Jeong JT, Moffatt HK (1992) Free-surface cusps associated with a flow at low Reynolds numbers. *J. Fluid Mech.* 241:1–22.
28. Lorenceau E, Restagno F, Quéré D (2003) Fracture of a viscous liquid. *Phys. Rev. Lett.* 90:184501.
29. Hinch EJ, Acrivos A (1979) Steady long slender droplets in two-dimensional straining motion. *J. Fluid Mech.* 91:401.
30. Hinch EJ, Acrivos A (1980) Long slender drops in a simple shear flow. *J. Fluid Mech.* 98:305.
31. Acrivos A, Lo TS (1978) Deformation and breakup of a single slender drop in an extensional flow. *J. Fluid Mech.* 86:641.
32. Pozrikidis C (1992) *Boundary Integral and singularity methods for linearized flow*. (Cambridge University Press, Cambridge).
33. Rallison JM (1984) The deformation of small viscous drops and bubbles in shear flows. *Annu. Rev. Fluid Mech.* 16:45.
34. Eggers J, Fontelos MA (2015) *Singularities: Formation, Structure, and Propagation*. (Cambridge University Press, Cambridge).
35. Doshi P, et al. (2003) Persistence of memory in drop breakup: the breakdown of universality. *Science* 302:1185.
36. Eggers J (2020) Theory of bubble tips in strong viscous flows.
37. Suryo R, Basaran OA (2006) Tip streaming from a liquid drop forming from a tube in a coflowing outer liquid. *Phys. Fluids* 18:082102.
38. Gañán-Calvo AM, González-Prieto R, Riesco-Chueca P, Herrada MA, Flores-Mosquera M (2007) Focusing capillary jets close to the continuum limit. *Nature Phys.* 3:737.

39. Pantano C, Gañán-Calvo AM, Barrero A (1994) Zeroth order, electrohydrostatic solution for electrospinning in cone-jet mode. *J. Aerosol Sci.* 25:1065.
40. Zhang WW (2004) Viscous entrainment from a nozzle: singular liquid spouts. *Phys. Rev. Lett.* 93:184502.
41. Castro-Hernández E, Campo-Cortés F, Gordillo JM (2012) Slender-body theory for the generation of micrometre-sized emulsions through tip streaming. *J. Fluid Mech.* 698:423.
42. Gradshteyn IS, Ryzhik IM (2014) *Table of Integrals Series and Products*. (Academic: New York).

473
474
475
476
477
478
479